

# A Computational-Graph Partitioning Method for Training Memory-Constrained DNNs

Fareed Qararyah  
Koç University, Turkey  
fqararyah18@ku.edu.tr

Mohamed Wahib  
National Institute of Advanced  
Industrial Science and Technology,  
Japan  
mohamed.attia@aist.go.jp

Doğa Dikbayır  
Michigan State University, USA  
dikbayir@msu.edu

Mehmet Esat Belviranlı  
Colorado School of Mines, USA  
belviranli@mines.edu

Didem Unat  
Koç University, Turkey  
dunat@ku.edu.tr

## Abstract

We propose PARDNN, an automatic, generic, and non-intrusive partitioning strategy for large DNN models that do not fit into single device memory. PARDNN decides a placement of DNN's underlying computational graph operations across multiple devices so that the devices' memory constraints are met and the training time is minimized. PARDNN is completely independent of the deep learning aspects of a DNN and requires no modification neither at the model nor at the systems level implementation of operation kernels. It partitions DNNs having billions of parameters and hundreds of thousands of operations in seconds to few minutes. Our experiments with TensorFlow on 16 GPUs demonstrate efficient training of 5 very large models while achieving superlinear scaling for both the batch size and training throughput. In comparison to related work (Mesh-TensorFlow and Gradient Checkpointing), PARDNN either outperforms or qualitatively improves upon them.

**Keywords** DNN, graph partitioning, model parallelism

## 1 Introduction

DNN models have doubled in size roughly every 2.4 years [16] and this growth is expected to continue in the coming years [2, 50]. Larger models, *deeper* or *wider* or both, produce results with higher accuracy on more complex tasks. However, they come at a high memory cost required to store the parameters and the intermediate results for both training and inference [53]. For example, in computer vision, considering Wide Residual Network [70], a widened variant of the well-known Resnet [19], widening the model 8 times increases the number of parameters  $\sim 60$  times [70] leading to a substantial increase in the memory requirements. The same trend shows up in the NLP field where deep-stacked LSTMs [66] or attention layers [61] often give more accurate results compared to shallower models but these newer models push the number of parameters up to  $O(10B)$  [50, 55].

Different approaches have been proposed to tackle the issue of training very large models on multiple devices. One

approach is to work on the model level, where the model is partitioned across multiple devices through model, pipeline, channel parallelism, or combinations of them [12, 15, 21, 27, 28, 43, 55]. Even though these methods are successful to some extent, they suffer from either: (a) being not generic as they target a specific class of DNNs, (b) introduce non-negligible memory overhead to maintain the statistical efficiency, or (c) can incur a high implementation cost and necessitate detailed understanding of the DNN model for an accurate cost model. Another approach works at the systems level by partitioning the computational graph that represents the operations in a neural network model and distributes it over multiple devices. However, the method proposed in [64] has a restricted applicability because it relies on a descriptive language to specify computations and cannot describe all the operations used in DL. Others propose a reinforcement learning-based approach, which is impractical in many cases due to substantial resource and time requirements [41, 42].

We adopt the system-level approach and propose a generic, efficient, and non-intrusive partitioning strategy (PARDNN) that avoids the drawbacks of the related work. PARDNN directly works on the computational graph representation of the neural network adopted by the most popular general-purpose DL frameworks such as TensorFlow [1] and MXNet [9]. Operating on the graph level has three main benefits. First, it provides a fine-grained view of the model, which gives more parallelization options and allows better load balancing and resource utilization. Second, it isolates our strategy from the details of the learning process, which provides more generality and guarantees unaffected statistical efficiency [43] of the model. Third, working at the level of the graph enables us to leverage decades of work on graph partitioning and static scheduling (as will be discussed later).

PARDNN's strategy is composed of two main steps. First, we cluster the operation-nodes of the computational graph into  $K$  partitions, where  $K$  represents the number of the available devices. The objective of this step is to reduce the end-to-end runtime by assigning the operations on the partitions such that the computational loads are balanced and the

communication is minimized. In the second step, we check whether the memory constraints are met in each partition. If they are not, we reassign some operations to different partitions such that the reassigned operations have the least possible perturbed effect on the placement generated by the first step but at the same time meet the memory constraints.

Most existing graph partitioning libraries are designed to handle undirected graphs. State-of-the-art graph partitioning tools, such as Scotch static mapper [45, 46] and MinCut optimizer, results in 2 to 10 times slowdown when applied on directed graphs of DL models [41, 42]. Our algorithm outline is inspired by the principle of the multilevel approach used in graph partitioning [30] but the design and algorithmic details of PARDDNN includes a mix of variants of static scheduling heuristics [31] that are mutated to reduce the time complexity, and novel techniques to address some shortcomings in the existing ones [40, 49]. Our contributions are:

- We propose a novel computational graph partitioning method that enables training models with large memory consumption on a set of devices with limited memory.
- We conduct extensive experiments with large DNNs to demonstrate PARDDNN’s efficiency. In comparison to related work: (a) PARDDNN’s performance is comparable to that of Mesh-TensorFlow, a state-of-the-art distributed training framework [54], while having qualitative advantages of automating the partitioning and not requiring model rewrite. (b) It generally outperforms redundant re-computation methods (Gradient Checkpointing [47]). (c) It outperforms out-of-core methods (CUDA Unified Memory).
- For models that do not fit into a single GPU’s memory, PARDDNN enables training models having up to 5.1 billion parameters using only 4 GPUs. For models that barely fit into a single device memory, it allows more efficient training by superlinearly scaling the batch size, and in many cases, the training throughput.
- PARDDNN’s overhead is negligible. For a graph having hundreds of thousands of nodes representing DNNs with billions of parameters, it takes  $\sim 2$  minutes to find a partition for 16 GPUs, while training these models takes days or even weeks.
- To the best of our knowledge PARDDNN is the first of its type that permits the training of models that do not fit into a single device memory while being generic due to (a) having zero dependency and requiring no knowledge about the DL aspects of the models, and (b) not requiring any modifications of the model or operation kernels.

## 2 Background

Many DL frameworks model a computation as a directed graph [1, 5, 9]. TensorFlow uses a stateful directed graph to represent the computational flow of operations. It extends the classical dataflow graph model to allow maintaining and

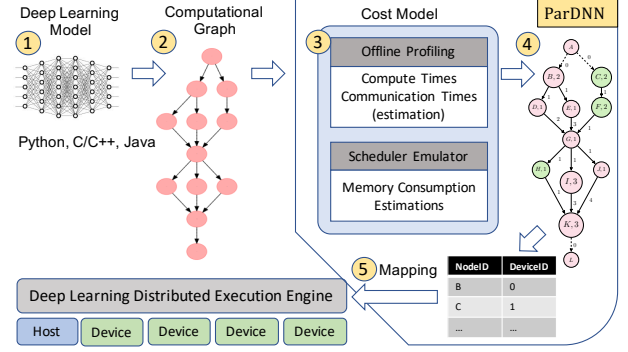


Figure 1. PARDDNN Overview

updating the persistent state of some special nodes, branching, and loop control. In a TensorFlow graph  $G = (V, E)$ , each node  $n \in V$  represents the instantiation of an operation (e.g., matrix multiplication or convolution) and it has zero or more inputs and zero or more outputs. Each edge  $e \in E$  represents a dependency between its incident nodes. Normal edges represent dataflow between the nodes, while special edges, e.g. control dependencies, are used to enforce happens-before relationships with no data flows along them [1].

Graph partitioning is, in general, defined as splitting the graph  $G(V, E)$  into  $K$  disjoint subsets [6]. The constrained version of the graph partitioning aims at partitioning in such a way that the sums of the vertices weights in each set are as equal as possible, and the sum of the weights of edges crossing between sets is minimized [30]. An extension of general graph partitioning which aims to assign a set of communicating tasks to processors is called *static mapping* [6]. Static mapping does not consider the logical and temporal dependencies of the tasks, it is assumed that all the tasks simultaneously coexist throughout the program execution.

Finding a spatial and temporal assignment of the set of nodes in a task graph  $G = (V, E)$  onto a set of processors resulting in the fastest possible execution, while respecting the precedence constraints expressed by all  $e \in E$  is referred to as task scheduling problem [56]. The schedule length, *makespan*, is the completion time ( $C_t$ ) of the last node in  $G$  assuming that the graph execution starts at time 0. The goal is to minimize  $C_{tmax}$ , where  $C_{tmax} = \max_{n \in V} C_t(n)$ . Finding an optimal schedule or static mapping is *NP-hard* [6, 56].

## 3 PARDDNN: A DNN Partitioning Strategy

PARDDNN offers a practical, non-intrusive, and generic method to partition a DNN on a set of processing elements (PE). The main objective of PARDDNN is to minimize  $C_{tmax}$ , the makespan of the computational graph, while satisfying the memory capacity constraints of the target processing elements. It is important to mention that PARDDNN does not have a runtime component. All the steps of PARDDNN are done ahead of time. After running PARDDNN once, the resulting partitioning can be used as long as the model parameters that affect the memory consumption do not change.

**Table 1.** Terminology used in this work

Term	Description
$G = (V, E)$	Computational graph with vertex set $V$ , edge set $E$
$CP$	Critical path of a graph
$C_{tmax}$	Makespan of $G$ , schedule length
$PE, pe$	Set of processing elements, a processing element
$K$	Number of processing elements (e.g., # of GPUs)
$comp(n)$	Weight of a node $n$ (compute time)
$mem(n)$	Memory consumption of outputs of a node $n$
$comm(e)$	Cost of an edge $e$ (communication time)
$sc$	Secondary cluster, which is a node or a path
$comm(sc)$	Total communication cost incurred by all edges that have one end in $sc$
$tl(n)$	Node top level: length of the costliest path between the source node of the graph and the node $n$ , excluding the node $n$ . Where the length of a path, is the summation of the computation costs of the nodes on the path and the communication cost of its edges $\sum_{n \in p} comp(n) + \sum_{e \in p} comm(e)$
$bl(n)$	Node bottom level: length of the costliest path between $n$ and the sink node including the node $n$
$w\_lvl(n)$	Node weighted level: $tl(n) + bl(n)$
$span(sc)$	Time between the expected finish time of the last parent of the first node in a $sc$ , and the expected starting time of the first child of the last node in that path. Last and first here mean topologically.
$potential(sc)$	Summation of the weights of all nodes that can be executed within $span(sc)$
$st(n)$	Starting time of node $n$ , the time when $n$ is assigned to a $pe$ to execute
$ft(n)$	Finish time of node $n$ , the time when $pe$ is done with executing $n$
$M_{cons}(pe, t)$	Memory consumed by the processing element at time $t$
$M_{pot}(n, t)$	Memory potential of a node $n$ at time $t$ . The summation of the memory occupied by the outputs of $n$ 's direct ancestors that are executed before $t$ , and for which $n$ is the last direct descendant in its $pe$ . Plus $n$ 's memory consumption if $st(n) \leq t \leq ft(n)$

Figure 1 shows the overall process. PARDNN takes a computational directed acyclic graph as an input, it annotates this graph with computation, communication, and memory consumption information gathered using offline profiling. PARDNN splits the graph into parts to be mapped to processing elements. PARDNN outputs the mapping information to be used by the execution engine of the DL framework (e.g. TensorFlow).

Our algorithm is divided into two major steps. Step-1 aims to obtain a partitioning that has a minimal makespan. Step-1 is further divided into three stages. Stage-I, *graph slicing* splits the graph into  $K$  disjoint primary and  $S$  disjoint secondary clusters. This splitting enables working at a coarser level in the upcoming stages. Stage-II, *mapping*, merges these  $S$  secondary clusters into the  $K$  primary clusters by firstly merging the clusters that have no parallelism gain, then merging the rest of  $S$  using a novel load balancing algorithm. The final stage of Step-1 is a *refinement* of the mapping through path swapping and node switching. In Step-2, the result from Step-1 is validated against the memory constraints of the given devices, if the constraints are satisfied, the partition will be the final output. Otherwise, the partition is refined until the memory consumption by a processing element  $pe$  at any time  $t \in [0, C_{tmax}]$  is less than or equal to  $pe$ 's memory capacity.

Next, we explain the details of each step. Table 1 summarizes the terms and notations used during explanations.

### Algorithm 1 Graph Slicing

---

**In :**  $K$ , Graph  $G$  ▷ number of devices, DNN graph  
**Out:**  $pri\_clusters[ ]$ ,  $sec\_clusters[ ]$  ▷ initially empty

---

```

1:  $j \leftarrow 1$ 
2:  $w\_lvls \leftarrow \text{compute\_weighted\_levels}(G)$ 
3: while  $G \neq \emptyset$  do
4:    $heaviest\_path \leftarrow \text{find\_heaviest\_path}(G, w\_lvls)$ 
5:   if  $j \leq K$  then
6:      $pri\_clusters[j] \leftarrow heaviest\_path$ 
7:      $w\_lvls \leftarrow \text{compute\_weighted\_levels}(G)$ 
8:   else
9:      $sec\_clusters[j - K] \leftarrow heaviest\_path$ 
10:  end if
11:   $G \leftarrow G - \{heaviest\_path\}$ 
12:   $j \leftarrow j + 1$ 
13: end while

```

---

### 3.1 Step-1: Partitioning To Minimize Makespan

Before presenting the details of the step, it is important to point its distinction from both static task scheduling and static mapping. Unlike scheduling algorithms, we do not specify an order of task execution; we rather focus on spatially allocating tasks on a set of processors while addressing the locality-parallelism trade-off. The order of execution decision is left to the runtime dynamic scheduler, e.g. TensorFlow scheduler. Unlike static mapping, PARDNN considers the logical and temporal dependencies between the tasks.

The size,  $(|V|)$ , of a DNNs' computational graph is usually in the order of hundreds of thousands and is projected to grow to millions of operation-nodes [50]. To have a scalable Step-1, we follow the concept of multilevel method [6], where we group vertices together and deal with groups of vertices, rather than individuals. This reduces the problem size and allows our heuristics to be applied within a reasonable time. Step-1 is designed in three main stages.

#### 3.1.1 Graph slicing

This stage groups the nodes of the graph into disjoint clusters. It iteratively finds the critical path ( $CP$ ) in the graph and removes  $CP$ 's nodes and their incident edges from the graph by marking them as visited so that they are not explored in the following iterations. This is repeated  $K$  times resulting in  $K$  primary clusters, which are the initial partitions assigned to different processing elements. Hence, the terms primary cluster and  $pe$  are going to be used interchangeably. After finding those primary clusters, if there are leftover nodes, we group them into secondary clusters. A secondary cluster, which is a linear cluster [56], is either a single node or a path. All the secondary clusters are identified and tagged until there is no node left on the graph that is not part of any cluster. Figure 2(b) shows an example.

Algorithm 1 shows the pseudo-code of the graph slicing, which takes  $K$  and graph  $G$  as inputs and outputs primary and secondary clusters. Line 2 computes the weighted level ( $w\_lvl(n)$ ) for all nodes in the graph. The heaviest path, (Line 4), is the  $CP$  when  $w\_lvl(n)$  are recalculated. Finding the

heaviest path is done by traversing the graph using the computed  $w.lvl$ s as priorities until reaching a dead-end. After forming a  $CP$ , it is added to the primary clusters and its nodes and edges are removed from the graph (Line 11). Unlike linear clustering [31], we obtain only  $K$  many  $CP$ s, then we stop recalculating  $w.lvl(n)$  for the secondary clusters since computing weighted levels is expensive. When weighted levels are not recalculated, *find\_heaviest\_path* may not return a  $CP$ , it rather returns a path of a heavy cost. This aims at capturing dependent and heavily-communicating nodes in the same cluster to increase locality. If a path could not be obtained, it returns a single node.

### 3.1.2 Mapping

This stage attaches the secondary clusters to the primaries with the objective of balancing the load among partitions and reducing communication. First, initial merging is applied to some of the secondary clusters for which executing them in parallel is not advantageous. For example, in Figure 2(c), the cluster  $\{J\}$  is merged with a primary because the total amount of communication ( $comm$ ) incurred by the nodes in cluster  $\{J\}$  can not be covered by its  $potential(\{J\})$ . Intuitively, the potential of a cluster measures how much parallel work is in the cluster at the time of its execution and whether or not that work is sufficient to totally hide its communication. In other words  $comm(\{J\}) - potential(\{J\}) > 0$ , hence there is no gain from assigning it to a distinct  $pe$ . Such a cluster is merged with the primary cluster with which it communicates the most.

Second, we apply a level-aware load balancing technique at which we merge the secondary clusters that are not merged by the initial merging. This process is referred to as *cluster mapping* in the scheduling literature. There are some heuristics such as wrap cluster merging [67], list scheduling based cluster assignment [52], and Guided Load Balancing (GLB) [49]. In a comprehensive evaluation of scheduling and cluster merging algorithms in [62], GLB is shown to produce the best result. However, GLB assumes that its preceding clustering step has eliminated the largest communication delays. As a result, the communication delays are not considered for cluster mapping [49]. Ignoring communication cost results in a low-quality mapping when the graph becomes very large. Even if each inter-cluster communication is small, the cumulative effect becomes considerable. In addition, the load balancing is global rather than time dependent (temporal). This issue is demonstrated in Figure 2(d) and (e). Ignoring the temporal aspect of load balancing causes GLB to make locally sub-optimal decision for cluster  $\{D\}$ . It assigns it to the less loaded  $pe$ , yet that  $pe$  has more work within the  $span(\{D\})$ . This assignment pattern is not suitable especially for TensorFlow graphs with frequent forks and joins, where the local and the global loads become more uncorrelated.

We propose a novel time-efficient heuristic called *Level-Aware Load Balancing (LALB)*. LALB considers both communication minimization and the temporal load balancing. We

### Algorithm 2 Mapping

---

**InOut:** pri\_clusters[ ] ▷ primary clusters  
**In:** sec\_clusters[ ] ▷ secondary clusters

---

```

1: for  $sc \in sec\_clusters$  do
2:   if  $comm(sc) - potential(sc) > 0$  then
3:      $target \leftarrow find\_most\_comm(sc, pri\_clusters)$ 
4:      $target \leftarrow target + \{sc\}$ 
5:      $sec\_clusters \leftarrow sec\_clusters - \{sc\}$ 
6:   end if
7: end for
8:  $comps[ ] \leftarrow \phi, comms[ ] \leftarrow \phi$ 
9: while  $sec\_clusters \neq \phi$  do
10:   $sc \leftarrow remove\_next\_secondary(sec\_clusters)$ 
11:   $comps \leftarrow calc\_work\_at\_span(span(sc), pri\_clusters)$ 
12:   $comms \leftarrow calc\_comms\_with(sc, pri\_clusters)$ 
13:   $target \leftarrow find\_minimal(comps, comms)$ 
14:   $target \leftarrow target + \{sc\}$ 
15: end while

```

---

temporally balance the loads by considering the workload of every  $pe$  within  $span(sc)$ , where  $sc$  is the secondary cluster that is going to be merged with one of the primary clusters.  $sc$  is mapped to a  $pe$  that has the minimal computational load within the  $span(sc)$ , and minimizes the incurred communication with the other processing elements. Equation (1) shows the selection criteria. In case of ties, we assign  $sc$  to the  $pe$  which has the highest communication value with it.

$$\min_{pe \in PE} \left( \sum_{\substack{n \in pe \\ tl(n) \in span(sc)}} comp(n) + \sum_{\substack{(n,u) \in E, \\ n \in \{PE\}-pe, \\ u \in sc}} comm(n,u) + \sum_{\substack{(u,n) \in E, \\ n \in \{PE\}-pe, \\ u \in sc}} comm(u,n) \right) \quad (1)$$

Algorithm 2 shows the two mapping procedures. Lines 1-7 do initial merging of the secondary clusters to the primaries. The while loop (Line 9) applies our novel load balancing. Most time is consumed in calculating the work in the span of the target secondary cluster  $sc$  (Line 11), in each of the primary clusters. We model this part as a problem of frequent range queries with updates. More specifically, we find the sum of the weights of the nodes whose levels fall in the span, and upon merging, the weights of those levels are updated. We use binary-indexed-trees [13] as a data structure, where the tree nodes store the weights per level. This data structure allows logarithmic range summation and value updates. Line 12 calculates the cost of communication between the secondary cluster  $sc$  in each of the primary clusters. Line 13 performs the selection criteria defined in Eqn (1) to select the best primary cluster to merge the  $sc$  with.

### 3.1.3 Refinement

This stage refines the partitioning with two refinement policies. The first is responsible for coarse-grained refinement at the secondary cluster level and the second does the fine-grained refinement at the node level. The first policy searches for a secondary cluster  $sc$  for which there is another secondary cluster  $sc'$  within its span that when swapped with  $sc$ , it results in better quality partitioning. The better quality comes from either enhancing the load balancing or reducing the total communication, or both.

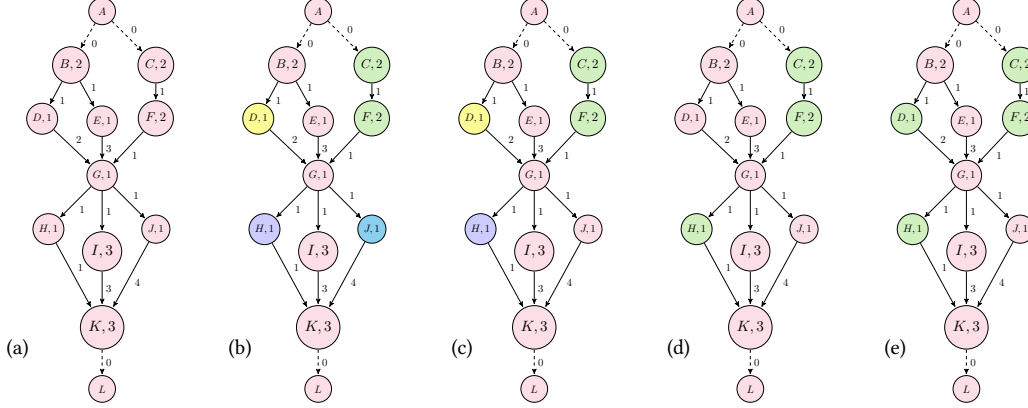


**Figure 2.** In the computational graph, vertex and edge weights indicate computation and communication costs, respectively. **(a)** Original computational graph, source node ( $A$ ) and sink node ( $L$ ) are added by PARDDN. **(b)** Shows the slicing stage when there are two  $pe(s)$ . Clusters are found in the following order:  $\{A, B, E, G, I, K, L\}$ ,  $\{C, F\}$ ,  $\{J\}$ ,  $\{D\}$ ,  $\{H\}$ . First two are primary clusters, the other three are secondaries. **(c)** Cluster  $\{J\}$  is merged to a primary cluster in initial merging since it has a communication of 5 units that cannot be hidden by the work within its span. **(d)** and **(e)** show LALB (ours) and GLB load balancing algorithms, respectively, after initial merging. The makespan of the LALB output is 13 units, while GLB is 15, thus LALB results in 15% performance gain.

The second policy handles a general issue with  $CP$  based heuristics that is discussed in [40]. This issue arises on the *communication-edges* among the processing elements. When there are many costly communicating operations in  $G$ , some of them may fall outside the  $CP$ . If their effect is large enough, they will create heavier  $CP$ s in the partitioned graph. Note that the  $CP$  of the graph after partitioning is probably different than the original  $CP$ . For example, in Figure 2(a) the  $CP$  is initially  $\{A, B, E, G, I, K, L\}$ , but after partitioning, the  $CP$  becomes  $\{A, C, F, G, I, K, L\}$  as in Figure 2(d). This is because the communication between the nodes in the same cluster is assumed to be zero. We repeatedly find the  $CP$  in the partitioned graph, as in Algorithm 1. Then we check the edges in that path that connect two different primaries, if moving a node incident to any of these edges to another primary shortens the  $CP$ , we switch that node’s primary. This process could be repeated as long as the  $CP$  can be shortened but since each time  $w\_lvals$  needs to be recalculated we choose to do it at most  $K$  times.

## 3.2 Step 2: Validating Memory Constraints

Similar to Step-1, we handle the memory constraints statically ahead of time for two reasons: (a) to avoid any runtime overhead and (b) to reduce the chance of conflicting with other runtime optimizations. Our approach is implemented separately from the memory management module of a DL framework, and could be seamlessly used with any dynamic optimization policies provided by the framework. Step-2 is further divided into three stages.

### 3.2.1 Scheduler Emulator

To address the memory consumption statically, temporal modeling of the allocation and deallocation patterns is required. Such modeling necessitates knowledge about scheduling in the DL framework to estimate when an operation

is going to start and finish execution. Consequently, when the memory allocated for the operation inputs is released and when a new memory is allocated to hold the operation outputs. To estimate those values, we emulate the TensorFlow scheduler. The TensorFlow scheduler maintains a ready queue that initially contains nodes with no ancestors. Each node has an in-degree representing the number of dependent nodes. The nodes are executed in FIFO order. Once a node is executed, the in-degrees of its children are decremented by one. Any node having an in-degree of zero will be pushed to the queue. Using the per-node running times and communication sizes collected from profiling, we emulate this behaviour to get the expected start- and end-times of the operations under a certain partitioning.

### 3.2.2 Tracking Memory Consumption

In TensorFlow, from the memory consumption perspective, operation-nodes broadly fall into three main categories. First, operations of which the data survives across iterations [1] and we refer to them as *residual nodes* ( $res\_ns$ ). Second, special operations that mutate the referenced tensor, of the first type, we refer to them as *reference nodes* ( $ref\_ns$ ). Those operations do not reserve any additional memory. However, they are co-located with the variables that they are mutating and must be moved together with their referred variable nodes. Third, operations that require additional memory proportional to their output size and we call them *normal nodes* ( $nor\_ns$ ). Memory for the output of these nodes is allocated upon scheduling and released once all their direct descendants are executed. This third type covers most of TensorFlow operations such as *matmul*, *conv*, and *add*. There is also temporary memory allocated for operation’s local variables. Those are immediately released once executed.

One might think that profiling solely peak memory footprints would be sufficient to predict the memory overflows.

However, to handle an overflow, nodes have to be moved between partitions and that in turn changes the schedule and the memory consumption at a certain time. Our cost model takes this dynamic behavior into account and models the interplay between the scheduler and memory usage.

$$M_{cons}(pe, t) = \sum_{\substack{n \in pe, \\ n \in res\_ns}} mem(n) + \sum_{\substack{n \in pe, \\ n \in nor\_ns, \\ st(n) \leq t \leq ft(n)}} mem(n) + \sum_{\substack{n \notin (pe \cap res\_ns), \\ ft(n) \leq t, \\ (n, u) \in E: st(u) \geq t, u \in pe}} mem(n) \quad (2)$$

Eqn (2) defines the memory consumption of a  $pe$  at time  $t$  as  $M_{cons}(pe, t)$ . The first term is the memory consumption of the  $res\_ns$  assigned to that  $pe$ . The second term indicates the memory consumption of the normal nodes that have started on that  $pe$  at  $\leq t$  and are being executed at  $t$ . The third indicates the nodes that have descendants assigned to that  $pe$  and the descendants' expected starting time is  $\geq t$ , and those nodes have finished at  $\leq t$  at any processing element except  $pe$ , or are non-residual that have finished at  $\leq t$  on that  $pe$ .

The overall memory consumption needs to be estimated for each node ( $|V|$  time points) because the change in memory consumption is triggered by node executions. Once a node starts executing, new memory space needs to be allocated and that may cause an overflow. Estimating memory consumption is done by visiting all the nodes in the graph in the order of their estimated starting times, which is obtained from the scheduler emulator, and keeping track of the accumulated memory consumption. In the same pass, the memory potential values of the nodes ( $M_{pot}$  in Table 1) are obtained. A node's memory consumption is added to the cumulative value once it is visited, and subtracted after its last descendent is visited unless it is a  $res\_ns$ .

### 3.2.3 Addressing Overflow

After estimating the memory consumption, we traverse the graph starting from the sink node and keep the nodes in a heap data structure, namely *nodes\_heap*. When the memory consumed exceeds the limit, we deal with the overflow as a 0-1 min-knapsack problem [11]. The min-knapsack problem is formulated as follows; given  $N$  pairs of positive integers ( $c_j, a_j$ ) and a positive integer  $O$ , find  $x_1, x_2, \dots, x_N$  so as to:

$$\text{minimize } \sum_{j=1}^N c_j x_j \quad \text{s.t. } \sum_{j=1}^N a_j \geq O \text{ and } x_j \in \{0, 1\} \quad (3)$$

In our case,  $O$  represents the amount of memory *overflow*, and  $a_j$  represents  $M_{pot}(n, t)$ . For the cost  $c_j$ , we use the summation of the node computation cost and the communication with its direct ancestors and descendants located on the same  $pe$ , as shown in Eqn (4), which defines *move\_cost*.

$$comp(n) + \forall u, v \in pe(n) \sum_{u:(u,n) \in G} comm(u, n) + \sum_{v:(n,v) \in G, v} comm(n, v) \quad (4)$$

**Table 2.** Complexity of Each Step of PARDNN

Step-1	Partitioning to Minimize Makespan
Graph Slicing (inc. sorting)	$O(K( V + E ))$
Mapping	$O( V  \cdot \log  V )$
Refinement	$O(K( V + E ))$
Step-2	Satisfying Memory Constraints
TensorFlow Scheduler Emulator	$O( V + E )$
Tracking Memory Consumption	$O( V )$
Addressing Overflow	$O( V ^2)$
Overall complexity of PARDNN	$O( V ^2)$

The idea behind *move\_cost* is that when a node is moved from a  $pe$  to another, it incurs a computational load imbalance proportional to its weight and extra communication proportional to its communication with the nodes assigned to the same  $pe$ . Our goal is to find a set of operation-nodes that the summation of their memory consumption potentials at the overflow time is  $\geq overflow$  when their total movement cost is minimized. The *movement criteria* is to pick the node with the lowest *move\_cost*/ $M_{pot}(n, t)$ . In other words we choose the node that alleviates the overflow while incurring the least amount of communication and computation imbalance.

The *nodes\_heap* is a min heap in which the *move\_cost* is the ordering key. To avoid choosing a node that has a low *movement criteria* but high *move\_cost*, each node for which the  $M_{pot}(n, t) > overflow$  is inserted in another heap at which the sorting key is *move\_cost*. When selecting, the top node is removed from both heaps and the one with the least *move\_cost* is chosen, and the other is returned to its heap. The selected node is moved to another  $pe$  if the target  $pe$  has sufficient memory to accommodate that node's memory potential. Otherwise, the node is not considered again and another node is picked from the heap. The algorithm terminates when either the overflow is completely eliminated or we run out of nodes without addressing it.

### 3.3 Time Complexity of PARDNN

Table 2 summarizes the time complexity of each step of PARDNN. Detailed explanations for the time complexities of each step can be found in Appendix A. The reported complexities after each step are relaxed ones and for some stages tighter bounds maybe driven with amortized analysis. Splitting the partitioning strategy into a set of simple, yet efficient, sub-stages permits lowering the complexity. The nodes are grouped into clusters in the first step, then for the most of later stages, PARDNN works at the cluster rather than node granularity, which considerably reduces the instance size it deals with. In practice, running PARDNN on the DNN models listed in Table 3 takes up to 2 minutes on a typical laptop processor, namely an Intel i7-7600u CPU @ 2.80GHz. Considering the training time of those models is in the orders of days or even weeks, PARDNN offers an extremely lightweight and practical approach to partition the computational graphs of DNNs.

## 4 Implementation

Our algorithm takes as an input the device count, their memory capacities, the interconnection bandwidth and latency



between them, the model computational graph, profiling data, operations metadata. The profiling data contain execution time measurements and the size of the output of each operation-node. The operation metadata contain the operation types (section 3.2.2s). TensorFlow standard APIs provide the profiling information including per-node time, memory consumption, and communication sizes at the granularity of graph nodes for regular as well as user-defined operators.

To estimate the memory consumption, we implemented an emulator of TensorFlow’s scheduler described in [1]. It is important to note that if PARDNN is intended to be used with another DL framework, another emulator can be written to emulate its scheduler, if needed, without modifying our partitioning algorithm. When handling memory constraints there is a trade-off between the overhead and the accuracy; static handling prioritizes overhead reduction over accuracy while dynamic handling targets the opposite. Due to the efficiency and maintainability reasons, we adopt the static approach. To accommodate sacrificing the exact details of the memory management optimizations and allocation details, such as fragmentation and temporary memory for local variables, we spare 10% of the device memory and constrain ourselves to the remaining 90%. This threshold was sufficient to successfully run all our experiments without going OOM. Nevertheless, this ratio might need to be tuned and it is the only parameter of PARDNN that needs tuning.

As shown in Figure 1, the output of our algorithm is a single file containing the operation placement as key-value pairs. Each key is an operation-node name and the value is the device on which the operation should be allocated. To control the placement at operation-node granularity, the TensorFlow back-end reads the node-to-device assignment from the placement file generated by our algorithm.

**PARDNN on multiple nodes:** Despite the capability of designing PARDNN to partition a DNN on multiple nodes, in this work we assume a single node where the processing elements are identical GPUs connected to a common host. This is because the number of GPUs per node has been steadily increasing over time. For instance, systems with 16 or more GPUs per node are in production (e.g. NVIDIA DGX SuperPOD). As suggested by many state-of-the-art works [21, 50, 55], we argue that a hybrid approach of data parallelism across compute nodes and using PARDNN inside the compute node is a practical choice. This approach benefits from the efficiency and non-invasiveness of our method in tackling the memory capacity issue at the node-level, while also harnessing the weak scaling properties of data parallelism across the nodes.

## 5 Results

This section is organized into three parts. First part compares the performance of PARDNN against related work: explicit model parallelism, redundant recompute, and an out-of-core method. The second part evaluates the scaling of PARDNN,

**Table 3.** Specifications of Models Datasets. (C)HSD: (Character) Hidden State Dimension, SL: Sequence Length, ED: Embedding Dimensions, RU: Residual Units, WF: Widening Factor, MD: Model Dimension, FS: Filter Size, P\_SZ: patch size.

Model / Dataset	Acronym	#Layers	HSD	SL	#Para. (10 <sup>9</sup> )	#Graph Nodes
RNN for Word-Level Language [58] / Tiny Shakespeare [29]	Word-RNN	8	2048	28	0.34	10578
	Word-RNN-2	8	4096	25	1.28	10578
Character-Aware Neural Language Models [32] / Penn Treebank (PTB) [38]	Char-CRN	8	CHSD	ED	0.23	22748
	Char-CRN-2	32	2048	15	1.09	86663
Wide Residual Net. [70] / CIFAR100 [34]	WRN	610	#RU	WF	1.91	187742
	WRN-2	304	101	14	3.77	79742
Transformer [61] / IWSLT’16 German-English corpus [8]	TRN	24	HSD	MD	1.97	80550
	TRN-2	48	5120	2048	5.1	160518
Eidetic 3D LSTM [65] / Moving MNIST digits [57]	E3D	320	FS	P_SZ	0.95	55756
	E3D-2	512	5	4	2.4	55756

and the last part performs overhead and fidelity analysis of PARDNN. Key findings of each part are as follows:

- **Comparison with Related Work:** (i) PARDNN achieves similar performance to the distributed tensor computation framework, Mesh-TensorFlow [54] but provides much higher user productivity. (ii) PARDNN outperforms Gradient Checkpointing [7] combined with data parallelism in many cases, yielding up to 2.8x speedup. More importantly, PARDNN enables training models where applying Gradient Checkpointing result in out of memory (OOM) even with a batch size of 1. (iii) PARDNN outperforms CUDA Unified Memory for all configurations and GPU counts.
- **Scaling:** (i) For the same number of GPUs, PARDNN enables the use of more than 9x batch size over the maximum possible with data parallelism on average. (ii) Superlinear speedup in most models and configurations is observed going from one GPU to 16 GPUs.
- **Overhead and Fidelity:** (i) Empirical overhead of PARDNN is no more than 2 minutes for the largest model over 16 GPUs. (ii) Replacing any of PARDNN steps with other heuristics or using alternative approaches result in significant drop in performance or huge increase in overhead, hence, demonstrating and justifying the design choices and efficiency of PARDNN’s algorithmic steps.

### 5.1 Environment, Models, and Datasets

We conducted all our experiments on a NVIDIA DGX-2 with 16 Tesla V100 SXM3 32GB GPUs connected via NVSwitch. The throughput measurements are conducted over the interval between the 100<sup>th</sup> and the 150<sup>th</sup> training iterations to get stable results. We use TensorFlow 1.14, and CUDA 10.0.

We experimented with five large models representing four main tracks of DL applications: image classification, translation, video prediction, and language modeling. All models and datasets used in experiments are listed in Table 3, and detailed in Appendix A. We focus our analysis on the performance of PARDNN, rather than pursuing the accuracy since

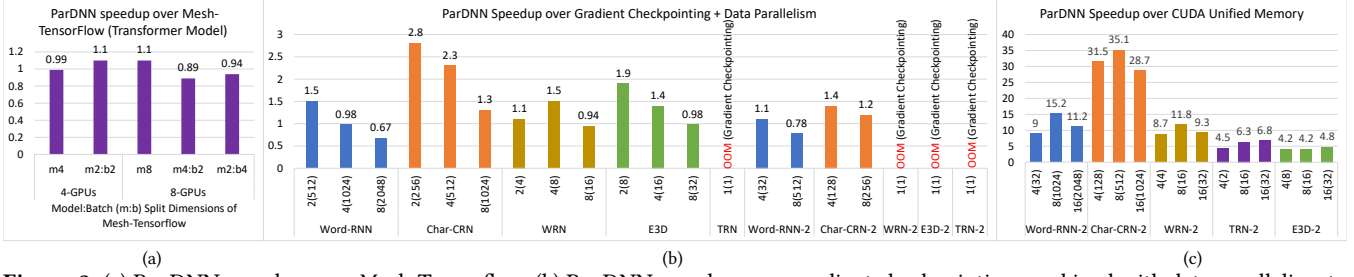


**Figure 3.** (a) PARDDN speedup over Mesh-Tensorflow, (b) PARDDN speedup over gradient checkpointing combined with data parallelism to run on multiple GPUs, (c) PARDDN speedup over CUDA Unified Memory (UM) using larger models. X-axis: Number of GPUs (Batch Size)

PARDDN has no effect on the learning aspect of the model: PARDDN does not alter the model nor its hyper-parameters.

## 5.2 Comparison with Related Work

We compare PARDDN to three different state-of-the-art approaches used to circumvent the memory limitation when training DNNs. We compare with (i) Mesh-TensorFlow [54] for explicit model parallelism, (ii) gradient checkpointing [7] in combination with data parallelism for redundant recompute and (iii) CUDA Unified Memory for out-of-core computing. Although there exists other graph-based solutions, we cannot directly compare either because we are not aware of any open source implementation [41] or the implementation is available for MXNet only [64]. It is worth mentioning, however, that PARDDN takes no more than 2 minutes for the largest configuration we tested, in comparison to 10s of hours reported by the other graph-based methods, in addition to PARDDN working on models 2.3x as large as what the other methods experimented with [41].

### 5.2.1 Mesh-TensorFlow

Mesh-TensorFlow [54], an extension to TensorFlow, was proposed to overcome the memory limitations of a single device and permits specifying a general class of distributed tensor computations. We compare the performance of PARDDN with Mesh-TensorFlow using the Transformer model which the original authors used to demonstrate the scaling [54]. Figure 3(a) shows the speedup of PARDDN over Mesh-TensorFlow using 4 and 8 GPUs. We report all permutations [60] possible with the maximum trainable batch size for Mesh-TensorFlow. PARDDN is on par with Mesh-TensorFlow, however, unlike Mesh-TensorFlow (a) PARDDN requires no knowledge about the DNN structure by the user, while with Mesh-TensorFlow it is the responsibility of the user to rewrite the model using Mesh-TensorFlow syntax. (b) PARDDN entirely automates the partitioning, while with Mesh-TensorFlow users have to manually specify the tensor-dimensions to be split across a multi-dimensional processor mesh and finding the best assignment is an NP-hard problem. (c) Mesh-TensorFlow has a non-negligible pre-run overhead which doubles when doubling the number of GPUs reaching  $\sim 1$  hour for 8 GPU assignment.

### 5.2.2 Redundant Recompute: Gradient Checkpoint

Gradient checkpointing [10] enables DNN training with a sublinear memory cost ( $O(\sqrt{N})$ ) when training an  $N$  layer network by recomputing the activations during backpropagation, instead of holding the forward pass results. In our comparison, we use a TensorFlow-based open-source implementation [7]. Figure 3(b) shows the speedup of PARDDN over gradient checkpoint when combined with data parallelism to run on multiple GPUs. For PARDDN and checkpointing, we used the common largest possible batch sizes. PARDDN outperforms gradient checkpointing in most cases. In few cases, checkpointing is better than PARDDN; this happens mainly when the degree of parallelism inherent in the graph is not sufficient to utilize all the GPUs. However, more importantly, PARDDN is qualitatively superior to gradient checkpointing since it enables the training of models where checkpointing fails to make them fit in device memory, even when using a batch size of one. For example, Figure 3(b) shows several configurations where gradient checkpointing goes out-of-memory at the batch size of one. Moreover, the overhead of gradient checkpointing can be up to 5 hours [7].

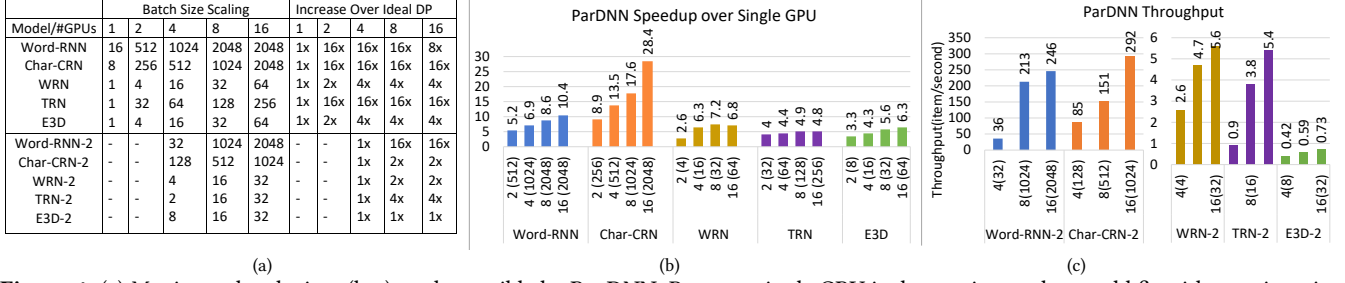
### 5.2.3 Out-of-core: CUDA Unified Memory

Figure 3(c) shows the speedup of PARDDN over CUDA Unified Memory (UM). UM, to the authors knowledge, is the only out-of-core solution that has an available TensorFlow implementation. In all cases, PARDDN throughput always improves going from 4 to 16 GPUs while increasing the batch size. UM performance in this case degrades when increasing the batch size due to the page faulting penalty [3].

## 5.3 Scaling Studies

We experimented with models under two main use-cases of PARDDN. First, model instances that *fit into a single device memory only with very small batch sizes*. Small here is relative to the numbers used by the DL community and reported in the literature. In such a case, PARDDN provides a qualitative advantage over data parallelism (DP), which splits the input over different GPUs that hold the replicas of the model. The second use-case is *model instances that do not fit into a single GPU memory even with small batch sizes*. These are larger variants of each model in Figure 4(a).





**Figure 4.** (a) Maximum batch sizes (bsz) made possible by PARDNN. Bsz on a single GPU is the maximum that could fit without triggering OOM. Table also shows the multiplier by which PARDNN could increase the bsz over ideal data parallelism (DP). For use-cases-1, DP is assumed to be applied on top of a single GPU reference point. For use-cases-2, PARDNN enables  $\geq 4$ -GPU assignment and DP is assumed to be applied on top of 4-GPU reference point. (b) PARDNN speedup over a single GPU using 2, 4, 8 and 16 GPUs. (c) Throughput and scaling up to 16 GPUs with larger models. In (b) and (c), batch size is shown in parenthesis.

### 5.3.1 Batch Size Scaling

Training with large batch sizes offers more parallelism and drastically reduces the overall training time. Authors in [17] proposed a method to scale batch sizes, which reduced the training of RESNET-50 on ImageNet to one hour. Another work harnessed very large batch sizes to reduce BERT training time from 3 days to 76 mins [69]. PARDNN enables super-linear scaling of the batch sizes while increasing the number of GPUs. Figure 4 (a) shows the batch size scaling for all of our experiments. We could increase the batch size by up to 256x for use-cases-1 and 64x for use-cases-2. This gives PARDNN a qualitative advantage even for models that fit into a single GPU since PARDNN enables training with much larger batch sizes than what can be achieved with DP.

PARDNN achieves superlinear scaling of the batch size firstly because with PARDNN, the parameters are not replicated but distributed. A large fraction of the memory consumed by the large models is to store the parameters and variables that survive through iterations. For instance, for 1.91 billion parameter WRN, TensorFlow allocates around 8GB for those variables. Using PARDNN these parameters are distributed, but with DP they need to be replicated. Secondly, for some operations, the memory consumption does not scale linearly with the batch size. For example, in *Word-RNN* and *Char-CRN*, the outputs of matrix multiplication operations have the largest memory consumption ratio. When doubling the batch size, the memory consumption by matrix multiplication results increases by only  $\sim 25\%$ . This is because the batch size might be the inner dimension for many of these multiplications, when multiplying a matrix of dimensions  $a \times \text{batch\_size}$  by another of  $\text{batch\_size} \times b$ , the result has the dimensions of  $a \times b$  regardless of the *batch\_size*. So the memory allocated to store the output of that operation does not increase, and this effect propagates to its decedents that will take its output as their input.

### 5.3.2 GPU Count Scaling

Figure 4(b) and (c) show the speedup over a single GPU for small models and the throughput scaling of PARDNN for large models, respectively, using the batch sizes in Figure 4.

In Figure 4(b), PARDNN shows a substantial improvement on 2 GPUs and a superlinear speedups up to 4 GPUs for all the models. The sharp performance increase happens because when a model fits into single GPU memory with small batch size, the resources are extremely underutilized. Pushing larger batches, while doubling the number of GPUs, improves the device utilization considerably. After 4 GPUs, the batch size could only be doubled when doubling the GPU count. The performance behavior beyond this point depends on inherent DoP (degree of parallelism) in the graph and CCR (the ratio of total communication cost to total computation cost) of the graph [44, 56]. Both *Word-RNN* and *Char-CRN* have large DoP, as a result, they continue to give superlinear speedups up to 8 and 16 GPUs, respectively. *TRN* exhibits modest improvement beyond 4 GPUs even though its graph has higher DoP in comparison to *WRN*. This is because it has a larger CCR (e.g. on 4-GPU configurations the CCR of *TRN* is 1.58 compared to 0.59 of *WRN*), hence a considerable amount of time is spent on communication. *E3D* scales better beyond 4 GPUs in comparison to *WRN* due to having higher DoP. However, the speedup, compared to a single GPU, is less because *E3D*'s main operation is 3D convolution, which heavily utilizes the GPU even with small batch sizes.

In Figure 4(c), going from 4 to 8 GPUs enables much larger batches in all cases but two. This in turn enhances the resource utilization and results in the substantial throughput improvements. *Char-CRN-2* perfectly scales up to 16 GPUs due to its high DoP. *Word-RNN-2* and *WRN-2* scale modestly from 8 to 16 because the batch size of 8 is sufficient to saturate the GPUs for *Word-RNN-2*. In case of *WRN-2*, the modest scaling is due to the low DoP.

## 5.4 Overhead and Fidelity of PARDNN

### 5.4.1 Overhead of PARDNN

PARDNN has a negligible overhead thanks to the low complexity of each step. The longest partitioning time among all the combinations of batch sizes, GPUs and model configurations used in this work was 117 secs in the case of partitioning *TRN-2* over 16 GPUs. The minimum time of 18 secs was taken to partition *Word-RNN* over 2 GPUs. Even though handling the memory overflow takes most of the

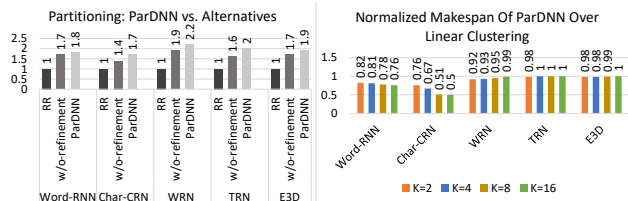


**Figure 5.** (a) PARDDNN’s speedup over Round Robin (RR) and ParDNN without refinement. The values are normalized over RR. Four GPU configuration is used. (b) Makespan of PARDDNN over that of Linear clustering (lower is better).  $K$  is the number of partitions.

overall partitioning time, the time taken to handle memory overflow is much lower than the theoretical upper bound. This is because Step-2 of PARDDNN depends on how many nodes need to be moved between clusters to address the overflow, which is much less than  $|V|$  in practice. The average ratio of the nodes moved in all our experiments is 8%.

#### 5.4.2 Analysis of PARDDNN Algorithmic Steps

To analyze the impact of slicing-mapping-refinement stages of Step-1, we replace Step-1 with a naive approach, which simply distributes the graph-nodes to the devices in a round-robin fashion (RR), where the nodes of the graph are iterated in their topological order. Figure 5(a) shows the performance improvement by PARDDNN over RR. In addition, the figure also shows the PARDDNN’s performance without the refinement. Compared to RR results, PARDDNN doubles the training throughput on average. Applying refinement has a non-negligible effect, contributing to 5-25% improvement.

#### 5.4.3 PARDDNN vs Linear Clustering

PARDDNN is not a standalone scheduling algorithm. It leaves the order of execution decision to the dynamic scheduler. However, it can still serve as an efficient phase in static scheduling. To show this feature and the advantage of our multi-staged approach over a high-complexity single heuristic, we compare PARDDNN with linear clustering (LC). To do a fair comparison, we implemented LC with GLB and Earliest Estimated Time First (EST First) [62] as a task ordering heuristic since this combination gave the best results. For PARDDNN, we used EST First as well to derive the execution order of tasks and omit the memory constraints (Step 2). Figure 5(b) shows that in all the experiments PARDDNN outperforms or is on par with LC. In particular, PARDDNN produces much better results than LC when the degree of parallelism is high as in *Char-CRN* and *Word-RNN*. Another advantage comes from the overhead. For the largest graph, *WRN* with  $\sim 190K$  nodes, it took PARDDNN 36 secs while LC took about 4.5 hours.

## 6 Related Work

**Systems-level approaches:** Mirhoseini et al. proposed a reinforcement learning-based method to place dataflow graphs on multiple devices [41, 42]. This approach suffers from significant time and resource consumption. The proposed

policy was trained for hours using 16 workers to produce placements for models having less than 100K operations. A more efficient approach was proposed by Wang et al. in [64]. However, it requires a description language to specify computations and cannot describe all the operations used in DL. Moreover, it partitions all operators and tensors across all workers, resulting in poor resource utilization.

**DL-level approaches:** Explicit model parallelism, where each worker is responsible for a subset of the layers, suffers from two major limitations: requiring complex cost models on case-by-case bases and leaving the partitioning burden to the programmer [43]. Pipeline parallelism provides good resource utilization yet some implementations requires a single layer to fit in a single device [22], which may not be the case for models with 3D inputs [39]. While in others, extra memory overhead proportional to the size of the model weights is necessary to address the statistical efficiency issue, i.e. preventing model convergence [43]. In [12, 27, 33, 55] non-generic techniques were proposed to parallelize specific types of DL models, some focusing on CNNs while others relying on Transformer in their optimizations.

**Virtualization and Recomputation:** methods relax the memory requirements. vDNN [51] is a memory manager that virtualizes GPU memory in DNN training. ooc\_cuDNN [25] extends cuDNN and applies cuDNN-compatible operators even when a layer exceeds GPU memory capacity by swapping at the granularity of individual tensor dimensions. Gradient checkpointing [10] reduces the memory needed to store the intermediate outputs and gradients with the cost of doubling the forward pass computational cost [10, 26]. Pooch [24] and Capuchin [47] propose a hybrid approach that selects either recomputing or swapping for certain layers to reduce the performance overhead based on profiling data.

**Graph partitioning:** To deal with a directed graph, existing graph partitioning libraries convert every directed edge to undirected even though this conversion loses crucial information [4]. Due to this reason, Scotch static mapper [45, 46] and MinCut optimizer, results in 2 to 10 times slowdown when applied on graphs of DL models [41, 42]. In [20], new techniques are proposed to deal with directed graphs and [44] built on top of those techniques for a clustering based scheduler. They aim at producing *acyclic partitioning*, where if there is a cut edge from partition  $a$  to  $b$  and another from  $b$  to  $a$ , the partition is considered cyclic, and is not acceptable. Since the graphs produced by Tensorflow are full of fork-joins, applying their technique to our DNN models results in unbalanced partitions.

**Static graph scheduling:** Plenty of sophisticated and high-quality algorithms were proposed [18, 23, 35, 36, 68] in this area. The vast majority of these algorithms were developed in 1990’s to handle small-sized graphs, and they were later evaluated using instances having up to 3000 nodes [14, 18, 37, 62, 63]. A recent evaluation on large graphs shows that

they either do not scale due to their high time-complexity, or produce low-quality allocations due to their inability to capture the global structure of the graph [44].

## 7 Conclusion

PARDNN presents a lightweight approach to partition computational graphs of very large DNN models. It permits the training of models that do not fit into a single device memory. The experiments on five large DNNs and comparisons with related work demonstrate its high efficiency and superlinear scaling of batch size and training throughput.

## Acknowledgement

Authors from Koç University are supported by the Turkish Science and Technology Research Centre Grant No: 118E801. This work was partially supported by JST-CREST under Grant Number JPMJCR19F5. The research presented in this paper has benefited from the Experimental Infrastructure for Exploration of Exascale Computing (eX3), which is financially supported by the Research Council of Norway under contract 270053.

## References

- [1] Martin Abadi, Ashish Agarwal, Paul Barham, Eugene Brevdo, Zhifeng Chen, Craig Citro, Greg S Corrado, Andy Davis, Jeffrey Dean, Matthieu Devin, et al. 2016. Tensorflow: Large-scale machine learning on heterogeneous distributed systems. *arXiv preprint arXiv:1603.04467* (2016).
- [2] Zahangir Alo, Tarek M. Taha, Chris Yakopcic, Stefan Westberg, Vasit Sagan, Mst Shamima Nasrin, Mahmudul Hasan, Brian C. Van Essen, Abdul A. S. Awwal, and Vijayan K. Asari. 2019. A State-of-the-Art Survey on Deep Learning Theory and Architectures. *Electronics* 8, 3 (2019), 292. <https://doi.org/10.3390/electronics8030292>
- [3] Ammar Ahmad Awan, Ching-Hsiang Chu, Hari Subramoni, Xiaoyi Lu, and Dhableswar K Panda. 2018. OC-DNN: Exploiting Advanced Unified Memory Capabilities in CUDA 9 and Volta GPUs for Out-of-Core DNN Training. In *2018 IEEE 25th International Conference on High Performance Computing (HiPC)*. IEEE, 143–152.
- [4] David A Bader, Henning Meyerhenke, Peter Sanders, and Dorothea Wagner. 2013. *Graph partitioning and graph clustering*. Vol. 588. American Mathematical Society Providence, RI.
- [5] James Bergstra, Frédéric Bastien, Olivier Breuleux, Pascal Lamblin, Razvan Pascanu, Olivier Delalleau, Guillaume Desjardins, David Warde-Farley, Ian Goodfellow, Arnaud Bergeron, et al. 2011. Theano: Deep learning on gpus with python. In *NIPS 2011, BigLearning Workshop, Granada, Spain*, Vol. 3. Citeseer, 1–48.
- [6] Charles-Edmond Bichot and Patrick Siarry. 2011. *Graph partitioning*. Wiley Online Library.
- [7] Yaroslav Bulatov. 2018. gradient-checkpointing. <https://github.com/cybertronai/gradient-checkpointing>.
- [8] Mauro Cettolo, Niehues Jan, Stüker Sebastian, Luisa Bentivogli, Roldano Cattoni, and Marcello Federico. 2016. The IWSLT 2016 evaluation campaign. In *International Workshop on Spoken Language Translation*.
- [9] Tianqi Chen, Mu Li, Yutian Li, Min Lin, Naiyan Wang, Minjie Wang, Tianjun Xiao, Bing Xu, Chiyuan Zhang, and Zheng Zhang. 2015. Mxnet: A flexible and efficient machine learning library for heterogeneous distributed systems. *arXiv preprint arXiv:1512.01274* (2015).
- [10] Tianqi Chen, Bing Xu, Chiyuan Zhang, and Carlos Guestrin. 2016. Training Deep Nets with Sublinear Memory Cost. *ArXiv abs/1604.06174* (2016).
- [11] János Csirik. 1991. Heuristics for the 0-1 min-knapsack problem. *Acta Cybernetica* 10, 1-2 (1991), 15–20.
- [12] Nikoli Dryden et al. 2019. Channel and Filter Parallelism for Large-Scale CNN Training. In *Proceedings of the International Conference for High Performance Computing, Networking, Storage, and Analysis (SC '19)*. Article 46, 13 pages.
- [13] Peter M Fenwick. 1994. A new data structure for cumulative frequency tables. *Software: Practice and experience* 24, 3 (1994), 327–336.
- [14] Apostolos Gerasoulis and Tao Yang. 1992. A comparison of clustering heuristics for scheduling directed acyclic graphs on multiprocessors. *Journal of parallel and distributed computing* 16, 4 (1992), 276–291.
- [15] Amir Gholami, Ariful Azad, Peter Jin, Kurt Keutzer, and Aydin Buluc. 2017. Integrated model, batch and domain parallelism in training neural networks. *arXiv preprint arXiv:1712.04432* (2017).
- [16] Ian Goodfellow, Yoshua Bengio, and Aaron Courville. 2016. *Deep learning*. MIT press.
- [17] Priya Goyal, Piotr Dollár, Ross Girshick, Pieter Noordhuis, Lukasz Wesolowski, Aapo Kyrola, Andrew Tulloch, Yangqing Jia, and Kaiming He. 2017. Accurate, large minibatch sgd: Training imagenet in 1 hour. *arXiv preprint arXiv:1706.02677* (2017).
- [18] Kun He, Xiaozhu Meng, Zhizhou Pan, Ling Yuan, and Pan Zhou. 2018. A novel task-duplication based clustering algorithm for heterogeneous computing environments. *IEEE Transactions on Parallel and Distributed Systems* 30, 1 (2018), 2–14.
- [19] Kaiming He, Xiangyu Zhang, Shaoqing Ren, and Jian Sun. 2016. Deep residual learning for image recognition. In *Proceedings of the IEEE conference on computer vision and pattern recognition*. 770–778.
- [20] Julien Herrmann, Jonathan Kho, Bora Uçar, Kamer Kaya, and Ümit V Çatalyürek. 2017. Acyclic partitioning of large directed acyclic graphs. In *2017 17th IEEE/ACM international symposium on cluster, cloud and grid computing (CCGRID)*. IEEE, 371–380.
- [21] Yanping Huang et al. 2018. GPipe: Efficient Training of Giant Neural Networks using Pipeline Parallelism. *CoRR abs/1811.06965* (2018). [arXiv:1811.06965](https://arxiv.org/abs/1811.06965)
- [22] Yanping Huang, Youlong Cheng, Ankur Bapna, Orhan Firat, Dehao Chen, Mia Chen, Hyukjoong Lee, Jiquan Ngiam, Quoc V Le, Yonghui Wu, et al. 2019. Gpipe: Efficient training of giant neural networks using pipeline parallelism. In *Advances in Neural Information Processing Systems*. 103–112.
- [23] Jing-Jang Hwang, Yuan-Chieh Chow, Frank D Anger, and Chung-Yee Lee. 1989. Scheduling precedence graphs in systems with interprocessor communication times. *SIAM J. Comput.* 18, 2 (1989), 244–257.
- [24] Yuki Ito, Haruki Imai, Tung D. Le, Yasushi Negishi, Kiyokuni Kawachiya, Ryo Matsumiya, and Toshio Endo. 2019. Profiling based out-of-core hybrid method for large neural networks: poster. *ArXiv abs/1907.05013* (2019).
- [25] Yuki Ito, Ryo Matsumiya, and Toshio Endo. 2017. ooc.cuDNN: Accommodating convolutional neural networks over GPU memory capacity. In *2017 IEEE International Conference on Big Data, Big-Data 2017, Boston, MA, USA, December 11-14, 2017*. 183–192. <https://doi.org/10.1109/BigData.2017.8257926>
- [26] Paras Jain, Ajay Jain, Aniruddha Nrusingha, Amir Gholami, Pieter Abbeel, Joseph Gonzalez, Kurt Keutzer, and Ion Stoica. 2020. Breaking the Memory Wall with Optimal Tensor Rematerialization. In *Proceedings of Machine Learning and Systems 2020*. 497–511.
- [27] Zhihao Jia, Sina Lin, Charles R Qi, and Alex Aiken. 2018. Exploring hidden dimensions in parallelizing convolutional neural networks. *arXiv preprint arXiv:1802.04924* (2018).
- [28] Zhihao Jia, Matei Zaharia, and Alex Aiken. 2018. Beyond Data and Model Parallelism for Deep Neural Networks. *CoRR abs/1807.05358* (2018). [arXiv:1807.05358](https://arxiv.org/abs/1807.05358) [http://arxiv.org/abs/1807.05358](https://arxiv.org/abs/1807.05358)

- [29] Andrej Karpathy. 2015. tinyshakespeare. <https://github.com/karpathy/char-rnn/tree/master/data/tinyshakespeare>
- [30] George Karypis and Vipin Kumar. 1995. Multilevel graph partitioning schemes. In *ICPP* (3). 113–122.
- [31] Sung J Kim. 1988. A general approach to multiprocessor scheduling. (1988).
- [32] Yoon Kim, Yacine Jernite, David Sontag, and Alexander M Rush. 2016. Character-aware neural language models. In *Thirtieth AAAI Conference on Artificial Intelligence*.
- [33] Alex Krizhevsky. 2014. One weird trick for parallelizing convolutional neural networks (2014). *arXiv preprint arXiv:1404.5997* (2014).
- [34] Alex Krizhevsky, Geoffrey Hinton, et al. 2009. Learning multiple layers of features from tiny images. (2009).
- [35] Yu-Kwong Kwok and Ishfaq Ahmad. 1995. Bubble scheduling: A quasi dynamic algorithm for static allocation of tasks to parallel architectures. In *Proceedings. Seventh IEEE Symposium on Parallel and Distributed Processing*. IEEE, 36–43.
- [36] Yu-Kwong Kwok and Ishfaq Ahmad. 1996. Dynamic critical-path scheduling: An effective technique for allocating task graphs to multiprocessors. *IEEE transactions on parallel and distributed systems* 7, 5 (1996), 506–521.
- [37] Jing-Chiou Liou and Michael A Palis. 1997. A comparison of general approaches to multiprocessor scheduling. In *Proceedings 11th International Parallel Processing Symposium*. IEEE, 152–156.
- [38] Mitchell Marcus, Grace Kim, Mary Ann Marcinkiewicz, Robert MacIntyre, Ann Bies, Mark Ferguson, Karen Katz, and Britta Schasberger. 1994. The Penn Treebank: annotating predicate argument structure. In *Proceedings of the workshop on Human Language Technology*. Association for Computational Linguistics, 114–119.
- [39] Amrita Mathuriya et al. 2018. CosmoFlow: Using Deep Learning to Learn the Universe at Scale. In *Proceedings of the International Conference for High Performance Computing, Networking, Storage, and Analysis (SC '18)*. IEEE Press, Piscataway, NJ, USA, Article 65, 11 pages.
- [40] CL McCreary, MA Cleveland, and AA Khan. 1996. The problem with critical path scheduling algorithms. *Master's Thesis, Department of Computer Science and Engineering Auburn University, USA* (1996).
- [41] Azalia Mirhoseini, Anna Goldie, Hieu Pham, Benoit Steiner, Quoc V Le, and Jeff Dean. 2018. A hierarchical model for device placement. (2018).
- [42] Azalia Mirhoseini, Hieu Pham, Quoc V. Le, Benoit Steiner, Rasmus Larsen, Yuefeng Zhou, Naveen Kumar, Mohammad Norouzi, Samy Bengio, and Jeff Dean. 2017. Device Placement Optimization with Reinforcement Learning. In *Proceedings of the 34th International Conference on Machine Learning - Volume 70 (ICML'17)*. JMLR.org, 2430–2439.
- [43] Deepak Narayanan, Aaron Harlap, Amar Phanishayee, Vivek Seshadri, Nikhil R Devanur, Gregory R Ganger, Phillip B Gibbons, and Matei Zaharia. 2019. PipeDream: generalized pipeline parallelism for DNN training. In *Proceedings of the 27th ACM Symposium on Operating Systems Principles*. 1–15.
- [44] M Yusuf Özkaya, Anne Benoit, Bora Uçar, Julien Herrmann, and Ümit V Çatalyürek. 2019. A scalable clustering-based task scheduler for homogeneous processors using DAG partitioning. In *2019 IEEE International Parallel and Distributed Processing Symposium (IPDPS)*. IEEE, 155–165.
- [45] François Pellegrini. 2009. Distillating knowledge about Scotch. In *Dagstuhl Seminar Proceedings*. Schloss Dagstuhl-Leibniz-Zentrum für Informatik.
- [46] François Pellegrini and Jean Roman. 1996. Scotch: A software package for static mapping by dual recursive bipartitioning of process and architecture graphs. In *International Conference on High-Performance Computing and Networking*. Springer, 493–498.
- [47] Xuan Peng, Xuanhua Shi, Hulin Dai, Hai Jin, Weiliang Ma, Qian Xiong, Fan Yang, and Xuehai Qian. 2020. Capuchin: Tensor-Based GPU Memory Management for Deep Learning. In *Proceedings of the Twenty-Fifth International Conference on Architectural Support for Programming Languages and Operating Systems (ASPLOS '20)*. Association for Computing Machinery, New York, NY, USA, 891–905. <https://doi.org/10.1145/3373376.3378505>
- [48] Alec Radford, Jeff Wu, Rewon Child, David Luan, Dario Amodei, and Ilya Sutskever. 2019. Language Models are Unsupervised Multitask Learners. *OpenAI Technical Report* (2019).
- [49] Andrei Radulescu and Arjan JC Van Gemund. 1998. GLB: A low-cost scheduling algorithm for distributed-memory architectures. In *Proceedings. Fifth International Conference on High Performance Computing (Cat. No. 98EX238)*. IEEE, 294–301.
- [50] Samyam Rajbhandari, Jeff Rasley, Olatunji Ruwase, and Yuxiong He. 2019. ZeRO: Memory Optimization Towards Training A Trillion Parameter Models. *ArXiv abs/1910.02054* (2019).
- [51] Minsoo Rhu, Natalia Gimelshein, Jason Clemons, Arslan Zulfiqar, and Stephen W Keckler. 2016. vDNN: Virtualized deep neural networks for scalable, memory-efficient neural network design. In *The 49th Annual IEEE/ACM International Symposium on Microarchitecture*. IEEE Press, 18.
- [52] Vivek Sarkar. 1988. Partitioning and scheduling parallel programs for execution on multiprocessors. (1988).
- [53] Taro Sekiyama, Takashi Imamichi, Haruki Imai, and Rudy Raymond. 2018. Profile-guided memory optimization for deep neural networks. *arXiv preprint arXiv:1804.10001* (2018).
- [54] Noam Shazeer, Youlong Cheng, Niki Parmar, Dustin Tran, Ashish Vaswani, Penporn Koanantakool, Peter Hawkins, HyoukJoong Lee, Mingsheng Hong, Cliff Young, Ryan Sepassi, and Blake Hechtman. 2018. Mesh-TensorFlow: Deep Learning for Supercomputers. In *Proceedings of the 32nd International Conference on Neural Information Processing Systems (NIPS'18)*. Curran Associates Inc., Red Hook, NY, USA, 10435–10444.
- [55] Mohammad Shoyebi, Mostofa Patwary, Raul Puri, Patrick LeGresley, Jared Casper, and Bryan Catanzaro. 2019. Megatron-lm: Training multi-billion parameter language models using gpu model parallelism. *arXiv preprint arXiv:1909.08053* (2019).
- [56] Oliver Sinnen. 2007. *Task scheduling for parallel systems*. Vol. 60. John Wiley & Sons.
- [57] Nitish Srivastava, Elman Mansimov, and Ruslan Salakhudinov. 2015. Unsupervised learning of video representations using lstms. In *International conference on machine learning*. 843–852.
- [58] Jack Jackson Sung Kim. 2017. Multi-layer Recurrent Neural Networks (LSTM, RNN) for word-level language models in Python using TensorFlow. <https://github.com/hunkim/word-rnn-tensorflow>
- [59] Ilya Sutskever, James Martens, and Geoffrey E Hinton. 2011. Generating text with recurrent neural networks. In *Proceedings of the 28th international conference on machine learning (ICML-11)*. 1017–1024.
- [60] Ashish Vaswani, Samy Bengio, Eugene Brevdo, Francois Chollet, Aidan N. Gomez, Stephan Gouws, Llion Jones, Lukasz Kaiser, Nal Kalchbrenner, Niki Parmar, Ryan Sepassi, Noam Shazeer, and Jakob Uszkoreit. 2018. Tensor2Tensor for Neural Machine Translation. *CoRR abs/1803.07416* (2018). <http://arxiv.org/abs/1803.07416>
- [61] Ashish Vaswani, Noam Shazeer, Niki Parmar, Jakob Uszkoreit, Llion Jones, Aidan N Gomez, Lukasz Kaiser, and Illia Polosukhin. 2017. Attention is all you need. In *Advances in neural information processing systems*. 5998–6008.
- [62] Huijun Wang and Oliver Sinnen. 2018. List-scheduling versus cluster-scheduling. *IEEE Transactions on Parallel and Distributed Systems* 29, 8 (2018), 1736–1749.
- [63] Jian Wang, Xinke Lv, and Xiao Chen. 2016. Comparative analysis of list scheduling algorithms on homogeneous multi-processors. In *2016 8th IEEE International Conference on Communication Software and Networks (ICCSN)*. IEEE, 708–713.
- [64] Minjie Wang, Chien-chin Huang, and Jinyang Li. 2019. Supporting very large models using automatic dataflow graph partitioning. In *Proceedings of the Fourteenth EuroSys Conference 2019*. 1–17.

- [65] Yunbo Wang, Lu Jiang, Ming-Hsuan Yang, Li-Jia Li, Mingsheng Long, and Li Fei-Fei. 2018. Eidetic 3d lstm: A model for video prediction and beyond. (2018).
- [66] Yonghui Wu, Mike Schuster, Zhifeng Chen, Quoc V Le, Mohammad Norouzi, Wolfgang Macherey, Maxim Krikun, Yuan Cao, Qin Gao, Klaus Macherey, et al. 2016. Google’s neural machine translation system: Bridging the gap between human and machine translation. *arXiv preprint arXiv:1609.08144* (2016).
- [67] Tao Yang. 1993. *Scheduling and code generation for parallel architectures*. Ph.D. Dissertation. Citeseer.
- [68] Tao Yang and Apostolos Gerasoulis. 1994. DSC: Scheduling parallel tasks on an unbounded number of processors. *IEEE Transactions on Parallel and Distributed Systems* 5, 9 (1994), 951–967.
- [69] Yang You, Jing Li, Sashank Reddi, Jonathan Hseu, Sanjiv Kumar, Srinadh Bhojanapalli, Xiaodan Song, James Demmel, Kurt Keutzer, and Cho-Jui Hsieh. 2019. Large batch optimization for deep learning: Training bert in 76 minutes. In *International Conference on Learning Representations*.
- [70] Sergey Zagoruyko and Nikos Komodakis. 2016. Wide residual networks. *arXiv preprint arXiv:1605.07146* (2016).

## A Appendix

### A.1 Time Complexity of Each Step of PARDNN

**Complexity of Graph Slicing:** The most expensive part of Algorithm 1 is computing weighted levels for all the nodes. This operation performs a variant of topological sorting and has time complexity of  $O(|V|+|E|)$  [56]. It is done  $K$  times, resulting in an overall complexity of  $O(K(|V|+|E|))$  as opposed to linear clustering that would cost  $O(|V|(|E|+|V|))$  [62].

**Complexity of Mapping:** Since the clusters are disjoint paths or singular nodes, and have no common nodes (a node exists only in one cluster), the total number of the update operations is bounded by  $|V|$ . The number of range summation queries is bounded by the number of the paths which is again bounded by  $|V|$ . The cost of either of the operations is logarithmic in the number of levels. The number of levels is  $\leq |V|$ , so we end up with  $O(|V|*log|V|)$ . Before starting LALB, we sort the clusters by their weights (the heaviest clusters first due to their importance in balancing the loads), this has an upper bound of  $O(|V|*log|V|)$ , since the number of clusters is upper-bounded by the number of nodes. Hence, the overall complexity of the mapping stage is  $O(|V|*log|V|)$ .

**Complexity of Refinement:** For swapping, initially we sort the clusters by  $tl(n)$  of their source nodes to find the clusters within the span of a certain cluster using binary search. Since the number of disjoint clusters is bounded by the number of nodes, this process gives the complexity of  $O(|V|*log(|V|))$ . Once two clusters are swapped, they are marked and not considered again leading to at most  $|V|$  cluster, hence node, swaps. With each swap the binary-indexed-trees are updated to reflect the new work loads. Since each update takes  $O(log(|V|))$ , overall complexity is  $O(|V|*log(|V|))$ . The node-level refinement is repeated  $K$  times and each time we recalculate the weighted levels and the  $CP$ . Upon node switching we update the trees. The overall time complexity is  $O(K(|V|+|E|))$ .

**Complexity of Scheduler Emulator:** The scheduler emulator estimates the starting time  $st(n)$  and finishing time  $ft(n)$  of the nodes in the graph. The emulator has time complexity of  $O(|V|+|E|)$ .

**Complexity of Tracking Memory Consumption:** Tracking the memory consumption requires  $O(|V|)$  time since it is done in one pass over the graph nodes while keeping the cumulative values and calculating the potentials.

**Complexity of Addressing Overflow:** We solve the knapsack greedily as the dynamic programming based solution complexity is impractical. When an overflow is detected, we pick the nodes from the heaps in a logarithmic time. Any node that is moved to another partition is guaranteed not to be moved again since it is moved only if the destination  $pe$  can accommodate it, meaning that it can neither cause nor solve an overflow on that  $pe$ . As a result, there is no repetition and a node can enter or exit the heap once, resulting in  $O(|V|*log|V|)$ . When a node is moved, the new potentials

and memory consumption need to be recalculated ( $O(|V|)$ ). It may happen at most  $|V|$  times. Overall the complexity is  $O(|V|^2)$ .

## A.2 Models and Datasets

From the language modeling, we use **Word-RNN** a multi-layer Recurrent Neural Network for word-level language inspired by the character-level modeling [59], and character-Aware Neural Language Models (**Char-CRN**) [32]. Both models can be enlarged by increasing the number of layers or the hidden state size. While Penn Treebank text corpus [38] is used to train **Char-CRN**, **Word-RNN** is trained using Tiny Shakespeare [29].

From computer vision, we experiment with **WRN** [70], which is a widened version of the residual network model. In **WRN** the width of the convolutional layers can be configured. The model size grows quadratically when widened. WRN has achieved better accuracy when the model is widened [70]. **WRN** is trained using **CIFAR** [34] as it is the dataset used by the original authors.

**TRN** (Transformer) [61] is a widely used model that had a significant influence on the design of SoTA Transformer-based models in the NLP domain such as GPT-2 [48] and Megatron-LM [55]. Transformer can be enlarged by increasing the number of layers, which deepens the model, and by widening the inner-layer dimensionality. Deeper [22] and wider [61] configurations of Transformer are shown to give higher accuracy. We trained Transformer using IWSLT 2016 German–English parallel corpus for training.

**E3D** is Eidetic 3D LSTM [65] for video prediction. This model achieves state-of-the-art performance in future frame prediction. *E3D* is closely related to convolutional recurrent networks, where the dimensions of memory states are increased, and 3D-Convs are adopted as the basic operators for state transitions. **E3D** can be enlarged by increasing the number of the hidden state channels on the memory dimensions. We trained E3D-LSTM using the Moving MNIST dataset.